ARTICLE

Check for updates

Journal of
Sensor Science and Technology

The Korean Sensors Society

Measurement of Electromagnetic Force of Pilot-Operated Type Solenoid Valve and Analysis of its Driving Characteristics

Min Jun Kim[1] and Hwa Young Kim[1,+]

[1]*School of Mechanical Engineering, Pusan National University M building 117, Pusan National University, 2, Busandaehak-ro 63 boen-gil, Geumjeong-gu, Busan 46241, Republic of Korea*

Cite This: *J. Sens. Sci. Technol. Vol. 35, No. 2 (2026) 121-129*

https://doi.org/10.46670/JSST.2026.35.2.121

ABSTRACT: This study investigates the electromagnetic characteristics of a pilot-operated solenoid valve employed in hydrogen storage systems, with a focus on the relationship between the air gap and electromagnetic force. The experimental setup consisted of a tensile-compression tester equipped with a digital push-pull gauge to measure the solenoid's electromagnetic force under various DC excitation voltages (8 V, 10 V, 12 V, and 14 V), with the air gap varying between 1.20 mm and 0.00 mm. The results demonstrated that as the air gap decreases, the magnetic flux density increases nonlinearly, resulting in a corresponding nonlinear increase in electromagnetic force. During the return stroke, the measured force was higher than during the approach stroke, indicating a dynamic hysteresis phenomenon caused by eddy currents generated during the change in the air gap. Finite Element Method (FEM) analysis using a 2D axisymmetric model showed similar trends; the magnetic flux density decreased from 1.32 T to 0.50 T as the air gap increased. Although the simulated forces were slightly higher than the experimental values due to unaccounted fringing flux effects in the model, the error remained within 5.00 N, confirming the model's reliability. These findings demonstrate that FEM-based static magnetic analysis can effectively predict the electromagnetic characteristics of hydrogen solenoid valves and offer a quantitative foundation for optimizing valve performance and design.

KEYWORDS: *Hydrogen storage system, Pilot-operated solenoid valve, Air gap, Electromagnetic force, Eddy current, Fringing flux (leakage flux)*

1. INTRODUCTION

A solenoid refers to a plunger type electromagnet that converts electrical energy into mechanical motion by energizing an AC or DC excitation coil to actuate a movable ferromagnetic core. A solenoid valve, in turn, is a general term for an automatic control valve that regulates pressure, flow rate, and flow direction by utilizing the magnetic field generated by electromagnetic force when current is applied to the coil [1].

In recent years, extensive studies have been conducted to quantitatively characterize the electromagnetic actuation behavior of solenoid valves and, based on such characterization, to optimize structural design and dynamic response. Choi, J. et al. investigated a pilot-operated solenoid valve for ultra-high-pressure vessels; they measured the actual motion of the plunger using a laser displacement sensor and an accelerometer, identified dynamic parameters including the damping coefficient, and modeled the multi-stage actuation behavior of the pilot valve [2]. Yang, L. et al. analyzed magnetic flux density and electromagnetic force for a high-speed solenoid valve used in an aircraft fuel system using the finite element method, and optimized the effects of design variables such as air gap length and core geometry on magnetostatic characteristics via the Taguchi method [3].

Meanwhile, Park, H.-J. et al. reported an evaluation of a direct-acting solenoid valve for hydrogen fuel cells, considering the increase in coil resistance due to heating and the resulting reduction in attractive force through coupled electromagnetic and heat transfer analyses [4]. In addition, studies have introduced models that account for magnetic hysteresis, particularly minor hysteresis loops, to improve the accuracy of thrust prediction for solenoid valves [5].

However, most prior studies have focused on oil/fuel

[+]Corresponding author: hyokim@pusan.ac.kr
Received : Feb. 5, 2026, Revised : Feb. 26, 2026, Accepted : Mar. 3, 2026

systems or direct-acting solenoid valves, or have primarily emphasized design optimization. As a result, relatively few studies have directly measured the dynamic electromagnetic force of a double plunger pilot solenoid valve used in hydrogen storage systems as a function of air gap variation, and systematically compared and validated the results against finite element analyses. Accordingly, this study investigates a double plunger type solenoid valve applied to a hydrogen storage system by experimentally measuring the attractive electromagnetic force as a function of air gap length and applied voltage, analyzing its dynamic characteristics, and comparing the results with a two-dimensional axisymmetric magnetostatic FEM analysis to quantitatively identify air-gap-dependent electromagnetic force characteristics and assess their reliability. If the electromagnetic force decreases in a hydrogen storage system due to external disturbances, delayed valve opening/closing can reduce fuel cell output; furthermore, if the hydrogen tank pressure exceeds the allowable limit, safety issues such as vessel rupture may occur.

To prevent such problems, it is necessary to measure electromagnetic force experimentally and to sufficiently analyze key variables that influence operation. In addition, to quantify these phenomena, it is necessary to analyze the magnetic field distribution and electromagnetic force under varying air gap conditions using the finite element method. Therefore, this study analyzes the electromagnetic force characteristics with respect to magnetic flux under a direct current (DC) condition and quantitatively discusses how these characteristics affect the actuation behavior of the solenoid valve. In this paper, magnetostatic analyses were performed by varying the solenoid air gap length using FEMM (Finite Element Method Magnetics), an electromagnetic field analysis program that is freely available and easy to use. The objective of the analysis is to quantitatively investigate changes in magnetic flux distribution, magnetic flux density, and electromagnetic force with respect to the air gap variation between the plunger and the core.

2. ELECTROMAGNETIC FORCE DESIGN OF A SOLENOID VALVE

2.1 Structure of a Solenoid Valve

The solenoid valve consists of a main plunger, a pilot plunger (movable core), a sol guide core (fixed core), a coil, and a sol housing, as shown in Fig. 1. When current is applied to the coil, a magnetic field is generated and an attractive force develops across the air gap, causing the plunger to be drawn toward and adhere to the core. The air gap region changes depending on whether current is applied to the solenoid, as

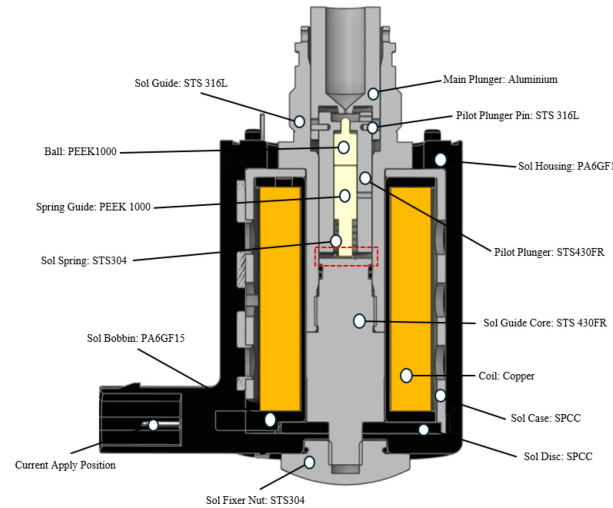

Fig. 1. Structure for a Pilot-Operated Solenoid Valve with corresponding materials

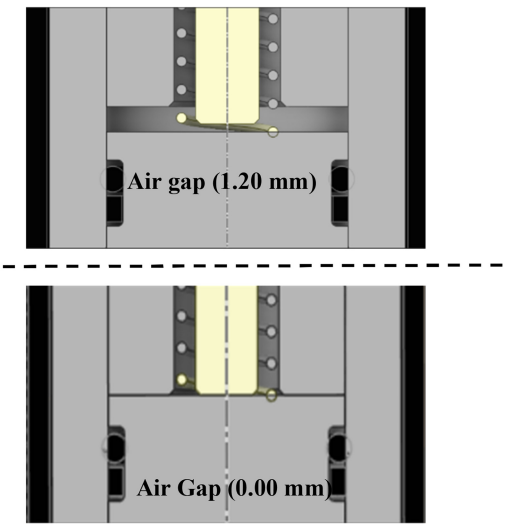

Fig. 2. Pilot-Operated Solenoid Valve Operation

indicated by the red box in Fig. 1 and illustrated in Fig. 2. When the electromagnetic force exceeds the spring force, the plunger moves by the air gap distance, resulting in a change in stroke.

2.2 Electromagnetic Model of a Solenoid Valve

The resistance of a solenoid varies with temperature. In this study, the solenoid temperature and resistance are assumed to be constant [6]. Under DC voltage excitation, the solenoid coil can be represented by the circuit shown in Fig. 3, where the resistance is constant; in steady-state, it can be modeled as an electrical circuit with constant inductance and current. According to Kirchhoff's voltage law, the voltage applied to the coil is equal to the sum of the voltage drop across the

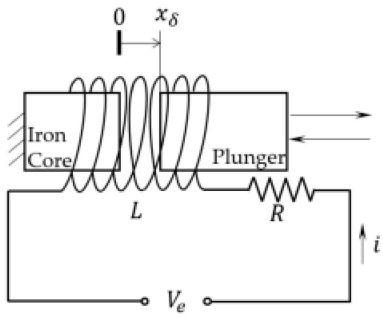

Fig. 3. RL circuit diagram

equivalent coil resistance and the electromotive force induced by the change in magnetic flux.

$$V_e = Ri + \frac{d\lambda}{dt} \tag{1}$$

Where, R is the ohmic resistance of the coil, i is the coil current, V_e is the applied voltage, and φ the total magnetic flux. The total flux linkage λ is defined based on the number of coil turns (N) and the total magnetic flux (φ), and is expressed as in Eq. (2).

$$\lambda = N\varphi \tag{2}$$

By substituting λ from Eq. (2) into Eq. (1), the applied voltage can be obtained as follows

$$V_e = Ri + N\frac{d\varphi}{dt} \tag{3}$$

The electromagnetic force F of a solenoid can be expressed, as shown in Eq. (4), as a function of the air gap flux density B_g, the absolute permeability μ_0 of air, and the cross-sectional area of the air gap region A_g. Where, the air gap flux density B_g can be written, as in Eq. (5), in terms of the relationship between the total flux linkage λ and the air gap cross-sectional area A_g. Substituting this expression into Eq. (4), the electromagnetic force can be reformulated as a relationship between the total flux linkage λ and the air gap cross-sectional area A_g [7,8].

$$F = \frac{B_g^2 A_g}{2\mu_0} \tag{4}$$

$$B_g = \frac{\lambda}{A_g} \tag{5}$$

Meanwhile, in this study, the electromagnetic force of the solenoid valve was described using a simplified quasistatic model in which the force is expressed as a function of the air gap flux density and the total magnetic flux. In actual valve actuation, however, Faraday's law implies that variations in coil current and changes in the air gap due to plunger motion cause the magnetic flux inside the core to vary with time. This time-varying flux induces an electric field within the core, generating eddy currents in closed loops. According to Lenz's law, these eddy currents produce a magnetic field that opposes the flux change, and the effect appears as a braking force acting opposite to the plunger's direction of motion. Accurately modeling eddy currents inside the core and plunger is difficult because many variables must be considered and their interactions are complex; thus, a rigorous analysis is not straightforward.

Therefore, this study adopts a model with simplifying assumptions and approximations, and the braking force is estimated by introducing appropriate approximations based on electromagnetic laws.

First, the expression is simplified by assuming that the coil has a single turn. Without this assumption, the expression for the total flux passing through the coil becomes a summation over the number of turns, which becomes highly complicated.

As a second simplification, the coil self-inductance is neglected. If it is not neglected, coupled differential equations containing two unknown functions the current $I(t)$ and the plunger velocity $v(t)$ must be solved, which significantly increases the complexity of the analysis. If $z(t)$ is defined as the distance from the coil center to the plunger, a simplified expression for the z-component of the magnetic field normal to the coil cross section can be written as in Eq. (6).

$$B_z(z(t)) = \frac{1}{z(t)^2 + C} B_0 \tag{6}$$

Where, B_0/C denotes the magnetic field at the plunger surface. The magnetic flux passing through the coil can then be expressed as in Eq. (7).

$$\varphi = \pi L^2 B_z(z(t)) \tag{7}$$

Where, L is the radius of the coil. Therefore, the induced EMF is given by Eq. (8).

$$\varepsilon = \frac{d\varphi}{dt} = \frac{d\varphi dz}{dz\,dt} = \pi L^2 \frac{dB_z(z)}{dz} v(t) \tag{8}$$

Where, $v(t) = dz/dt$ denotes the translational velocity of the plunger. Using another rough approximation, the expression can be written as in Eq. (9).

$$\frac{dB_Z(z)}{dz} = C' \tag{9}$$

In other words, this expression is written by treating it as a constant C'. However, in practice, it is not a constant; it varies with time t and can be interpreted as the time-averaged value of dB_Z/dz. In addition, if the coil self-inductance is neglected, the current flowing through the coil

can be expressed as in Eq. (10).

$$I = \frac{\varepsilon}{R} = \pi L^2 C' \frac{v(t)}{R} \tag{10}$$

According to the Lorentz force, the force exerted by the plunger on the coil is given by Eq. (11).

$$F = \int I d\vec{l} \times \vec{B} \tag{11}$$

Where, $\vec{B}$ is the total magnetic field generated by the plunger at each coil winding position, and $d\vec{l}$ is an infinitesimal length vector along the current-carrying path of the coil. The magnetic field can be expressed as $\vec{B} = B_x\tilde{X} + B_y\tilde{Y} + B_z\tilde{Z}$, which has x-, y-, and z- components. Evaluating the integral shows that the net force due to the z-component $B_z(z)$ is always zero; therefore, it is sufficient to compute only the integrals associated with the x- and y-components of $\vec{B}$. We further make the simplifying assumption that those x- and y- components are such that their sum $\vec{B}_N = B_x\tilde{X} + B_y\tilde{Y}$ is normal to the $d\vec{l}$. With this assumption, the expression can be rearranged as in Eq. (12).

$$F = \int \vec{B_N} I d\vec{l} = 2\pi L \vec{B_N} I = 2\pi^2 \frac{L^3 C' \vec{B_N}}{R} v(t) \tag{12}$$

Therefore, the braking force acting on the plunger can be expressed, according to Newton's third law, as $-F$.

3. EXPERIMENTAL SETUP AND PROCEDURE

3.1 Electromagnetic Force Test Setup

Fig. 4 illustrates the configuration of the electromagnetic force test setup. A digital push-pull gauge is connected to a tensile-compression testing machine, and the main plunger is fastened to a threaded attachment of the push-pull gauge. The tensile force measured by the load cell is converted to electromagnetic force (N) and displayed as a digital value. The data measured by the load cell are transmitted by connecting the USB port of the tensile-compression testing machine to a desktop computer, and the results can be monitored as graphs via the measurement software (Force Recorder Professional) synchronized with the load cell digital output. The stroke between the plunger and the core is adjusted using a ball-screw-driven vertical translation stage that moves the load cell up and down. In addition, a fixing jig and an angle adjuster capable of tilting and rotating were used to secure the solenoid valve and to ensure coaxial alignment between the core and the plunger.

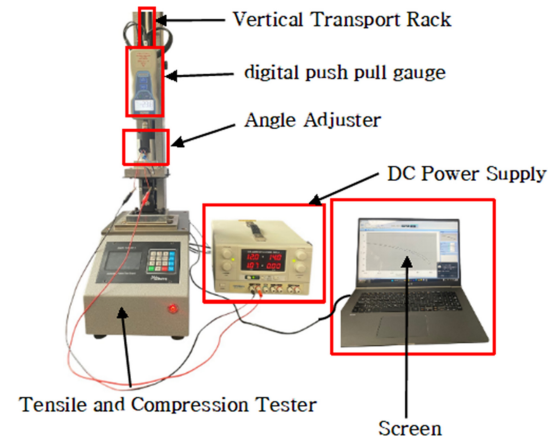

Fig. 4. Experimental setup for electromagnetic force measurement

3.2 Experimental Conditions and Methods

Using a DC power supply, constant voltage (CV) levels of 8 V, 10 V, 12 V, and 14 V were applied to the solenoid valve coil. The experiment was initiated at an air gap distance of 1.20 mm, and the translation stage was driven at a feed rate of 5.00 mm/min under a vertical reciprocating motion of 2.40 mm. The sampling frequency of the measurement program was set to 10 Hz. All measurements were repeated three times for each condition, and the average values were reported. To measure the intrinsic electromagnetic force, the ball, spring guide, and spring were removed during the experiments.

4. RESULTS AND DISCUSSION: EXPERIMENTS AND SIMULATIONS

4.1 Experimental Results of Electromagnetic Force Measurements with Varying Air Gap Distance

In this experiment, the electromagnetic force of a solenoid actuator was measured as a function of air gap variation. The results showed an asymmetric behavior: compared with the air-gap-decreasing interval (1.20 mm → 0.00 mm) shown in Table 1. and Fig. 5, the electromagnetic force at the same air gap was higher in the subsequent air-gap-increasing interval (0.03 mm → 1.20 mm) shown in Table 2. and Fig. 6. This phenomenon can be interpreted as a dynamic hysteresis effect induced by eddy currents generated during the air gap transition process.

Therefore, the underlying mechanism is discussed theoretically below. As the air gap changes, the magnetic flux distribution inside the plunger and the core varies with time. In electrically conductive metallic cores and plungers, a flux-change-rate-dependent induced electromotive force is generated, which leads to the formation of eddy currents.

Table 1. Electromagnetic Force Analysis Results for Downward Motion

Air Gap	8 V	10 V	12 V	14 V
0.00 mm	42.8 N	46.1 N	47.0 N	49.3 N
0.10 mm	33.3 N	37.4 N	40.7 N	42.4 N
0.20 mm	27.8 N	32.0 N	35.0 N	37.4 N
0.30 mm	23.1 N	27.6 N	30.9 N	33.3 N
0.40 mm	19.7 N	24.5 N	27.7 N	30.3 N
0.50 mm	16.6 N	21.8 N	25.1 N	27.7 N
0.60 mm	14.5 N	19.4 N	22.8 N	25.4 N
0.70 mm	12.7 N	17.4 N	20.8 N	23.4 N
0.80 mm	11.2 N	15.5 N	19.0 N	21.6 N
0.90 mm	10.0 N	14.1 N	17.3 N	20.1 N
1.00 mm	9.03 N	12.7 N	15.9 N	18.7 N
1.10 mm	8.33 N	11.6 N	14.6 N	17.4 N
1.20 mm	7.76 N	10.9 N	13.7 N	16.4 N

Table 2. Electromagnetic Force Analysis Results for Upward Motion

Air Gap	8 V	10 V	12 V	14 V
0.03 mm	43.3 N	46.3 N	48.7 N	50.0 N
0.10 mm	36.5 N	39.2 N	42.6 N	44.4 N
0.20 mm	29.2 N	33.2 N	36.0 N	38.1 N
0.30 mm	24.6 N	28.6 N	31.6 N	33.8 N
0.40 mm	20.5 N	25.1 N	28.0 N	30.1 N
0.50 mm	17.7 N	22.4 N	25.4 N	27.6 N
0.60 mm	15.3 N	20.0 N	23.3 N	25.2 N
0.70 mm	13.4 N	18.0 N	21.6 N	23.4 N
0.80 mm	11.8 N	16.1 N	19.5 N	21.7 N
0.90 mm	10.6 N	14.6 N	17.9 N	20.3 N
1.00 mm	9.53 N	13.3 N	16.5 N	18.8 N
1.10 mm	8.70 N	12.2 N	15.4 N	17.8 N
1.20 mm	8.20 N	11.3 N	14.3 N	16.8 N

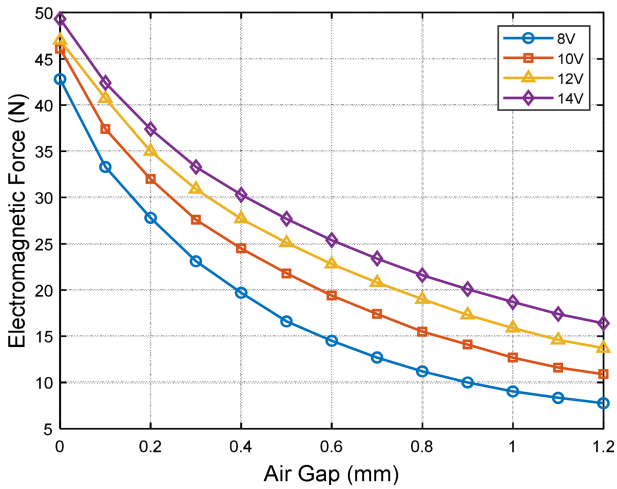

Fig. 5. Electromagnetic Force-Air Gap Curves for Downward Motion

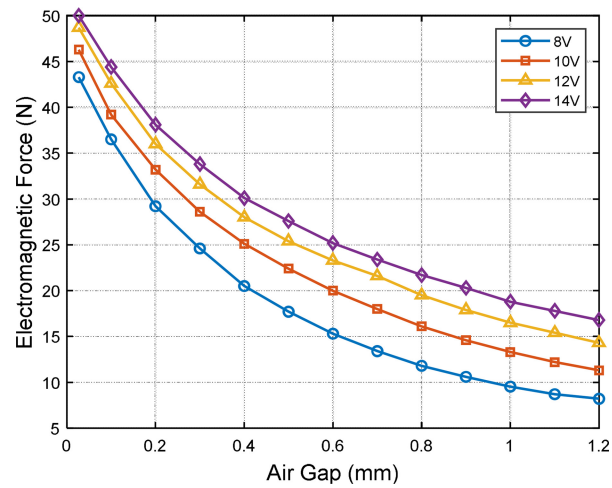

Fig. 6. Electromagnetic Force-Air Gap Curves for Upward Motion

According to Lenz's law, these eddy currents produce a magnetic field that opposes the flux change, thereby tending to delay the rate of increase or decrease of the actual air gap flux. Consequently, during the air-gap-decreasing interval, eddy currents suppress the increase in magnetic flux, resulting in a relatively lower effective flux and electromagnetic force at a given air gap.

Conversely, during the air-gap-increasing interval, eddy currents suppress the decrease in magnetic flux, allowing the flux to persist for a longer time and thus producing a larger electromagnetic force at the same air gap. This behavior is also consistent with the fact that a time-varying magnetic field penetrates a conductor via magnetic diffusion, and an effective time constant is determined by the material permeability and electrical conductivity.

In other words, even at the same air gap, the force can differ depending not only on the instantaneous air gap value but also on the direction (decreasing/increasing) and the rate at which the air gap is reached. The hysteresis error shown in Fig. 7 is summarized in Table 3. The error varied with both air gap and applied voltage; for example, at an air gap of 0.10 mm, the hysteresis error under the 8 V condition was the largest, reaching 9.00%. In contrast, at an air gap of 0.70 mm under 14 V, the hysteresis error was 0.00%, indicating that the difference between the increasing and decreasing intervals was negligible. Overall, relatively larger errors tended to appear in the intermediate air gap range of approximately 0.10–0.60 mm. This can be explained by the fact that the flux change rate

Table 3. Hysteresis Analysis Results for Upward Motion and Downward Motion

Air Gap	8 V Hysteresis Error	10 V Hysteresis Error	12 V Hysteresis Error	14 V Hysteresis Error
0.10 mm	9.00%	5.08%	5.42%	5.95%
0.20 mm	3.93%	3.38%	2.85%	2.08%
0.30 mm	4.22%	2.82%	2.00%	1.48%
0.40 mm	2.25%	1.69%	0.85%	0.59%
0.50 mm	3.09%	1.69%	0.85%	0.29%
0.60 mm	2.25%	1.69%	1.42%	0.59%
0.70 mm	1.96%	1.69%	2.28%	0.00%
0.80 mm	1.68%	1.69%	1.42%	0.29%
0.90 mm	1.68%	1.41%	1.71%	0.59%
1.00 mm	1.40%	1.69%	1.71%	0.29%
1.10 mm	1.04%	1.69%	2.28%	1.19%
1.20 mm	1.23%	1.12%	1.71%	1.19%

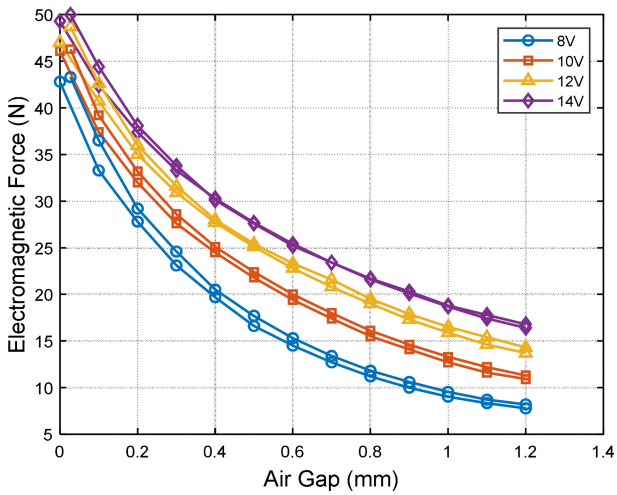

Fig. 7. Hysteresis Analysis Results for Upward Motion and Downward Motion

and the degree of magnetic diffusion within the conductor differ across air gap ranges.

Specifically, at large air gaps, the flux magnitude is small, and the change rate is limited, whereas at very small air gaps, even if the flux increases, the force sensitivity to further changes may become relatively mild; as a result, the eddy current effect may manifest more prominently as a force difference in the intermediate air gap region [9,10].

In addition, regression analysis of the electromagnetic force data in the two intervals confirmed that the force can be approximated by a second-order polynomial function of the air gap, as shown in Fig. 5 and Fig. 6. This quantitatively demonstrates the nonlinear characteristics of the electromagnetic force curve with respect to air gap variation, and the resulting approximation can be used as a surrogate model for subsequent comparison with FEM results and for predicting actuation characteristics.

4.2 Results of Magnetostatic FEM Analysis

Although the electromagnetic force of a solenoid can be calculated using Eq. (4), accurately predicting its exact value is difficult. This is because it is challenging to fully account for the leakage flux generated in the solenoid, and it is not straightforward to quantify the loss of electromagnetic force caused by eddy currents. Therefore, it is common to estimate the electromagnetic force through electromagnetic field analysis using FEM software.

In this study, the analysis was performed under steady-state conditions with no time variation of magnetic flux, using a two-dimensional axisymmetric model. The model consisted of the core, plunger, coil, and surrounding air region, and the coil was assigned a current of 0.8 A and 1148 turns. The core material was set to STS430FR, and magnetic saturation was taken into account by inputting the nonlinear B–H curve of the material, as shown in Fig. 8. In a solenoid, the magnetic flux path changes with the air gap distance, and the leakage flux distribution changes accordingly.

In this section, FEM analyses were conducted for each valve stroke (air gap distance) to obtain the magnetic flux density and electromagnetic force, and the air-gap-dependent electromagnetic force characteristics were compared with and analyzed against the experimental results. Fig. 9 shows the air-gap-dependent magnetic flux density distributions obtained from the FEMM analysis. It can be confirmed that the flux is concentrated around the air gap region between the core and the plunger, and the air gap flux density exhibits a nonlinear decrease as the air gap distance increases, as shown in Fig. 10.

As presented in Table 4. and Fig. 11, when the electromagnetic force acting on the plunger was measured separately during the air-gap-decreasing (descending) and air-gap-increasing (ascending) interval, and the average value was used, the FEM-predicted forces were generally higher than the experimental values. This is because the 2D axisymmetric FEM model, defined about the model axis, cannot adequately capture (i) the leakage flux occurring on the side of the housing near the power supply unit and (ii) the leakage flux associated with the fluid flow passage machined on one side of the plunger. As a result, the experimentally measured force tends to be lower than the simulated value [11].

As shown in Fig. 9(a), when the air gap distance is around 0.10 mm, the flux density in the core-plunger air gap region increases to approximately 1.32 T, entering the pre-saturation

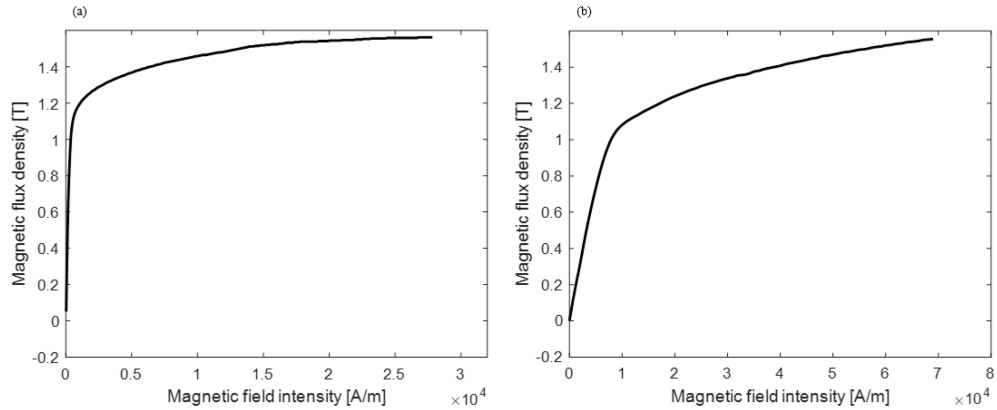

Fig. 8. Magnetic flux density versus magnetic field intensity for (a) STS430FR and (b) SPCC.

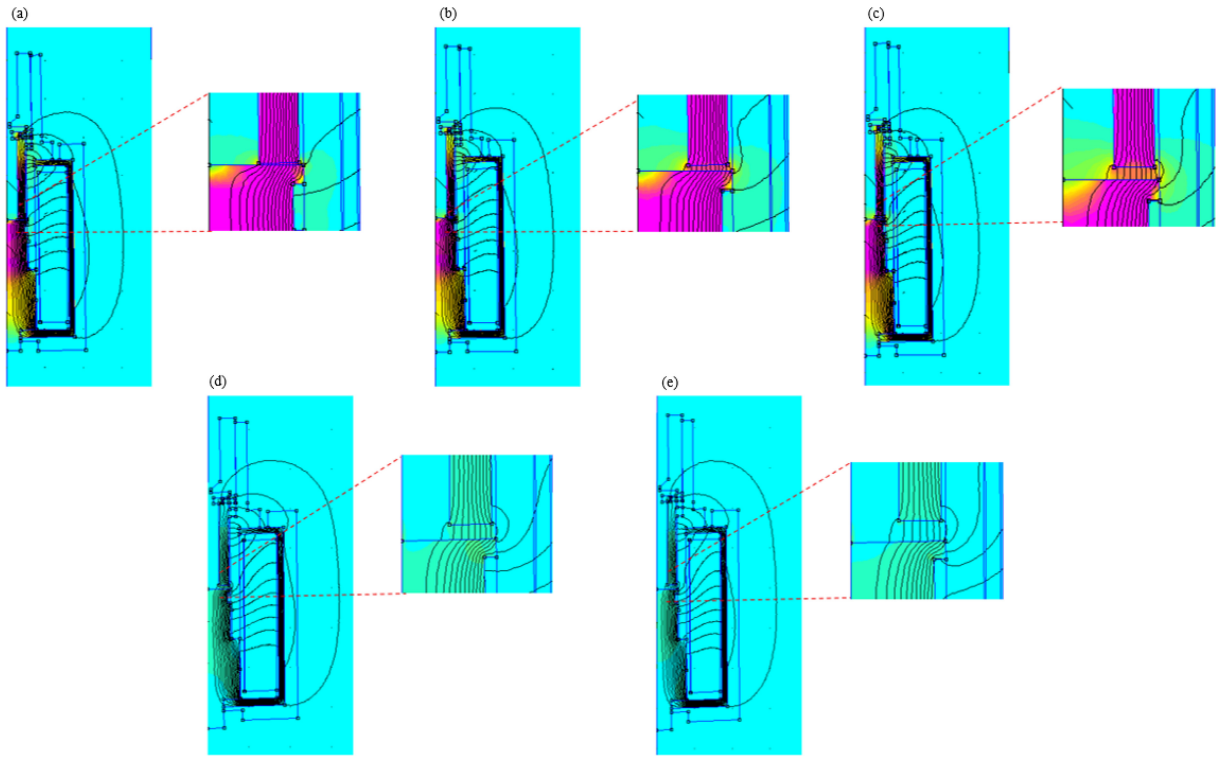

Fig. 9. Magnetic Flux Flow Comparison for Different Stroke Positions. (a) Air gap is 0.10 mm, (b) Air gap is 0.30 mm, (c) Air gap is 0.60 mm, (d) Air gap is 0.90 mm and (e) Air gap is 1.20 mm

region on the B–H curve of STS430FR. In this pre-saturation region, the slope of the B–H curve changes rapidly due to permeability variations, and local flux concentration, and three-dimensional changes in flux distribution can occur near the plunger edge. Therefore, even with a nonlinear B–H curve, a 2D axisymmetric model cannot fully reproduce the flux distribution and saturation behavior of the actual three-dimensional structure [12]. Consequently, at an air gap distance of (a) 0.10 mm, the experimental force was 34.9 N while the FEM result was 39.8 N, yielding an absolute error of 4.90 N (relative error of 14.0%), which was the largest discrepancy among the tested points.

In contrast, in regions where the air gap increases (e.g., (b) 0.30 mm~(e) 1.20 mm), most of the magnetic flux forms a closed magnetic circuit through the core-plunger path, so the influence of material nonlinearity becomes relatively smaller. As the air gap length increases, the magnetic reluctance of the air gap increases and the proportion of fringing and leakage flux increases; however, the overall flux level and the electromagnetic force decrease. Moreover, in a 2D axisymmetric model, if a sufficiently large air region and appropriate boundary conditions are applied, the fringing flux

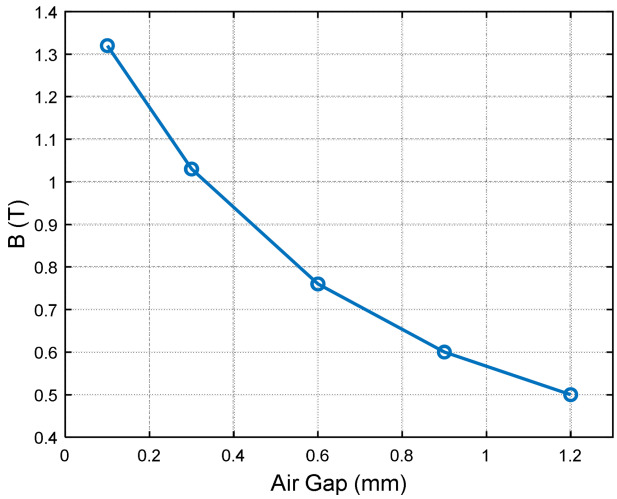

Fig. 10. Variation of air gap magnetic flux density with air-gap distance

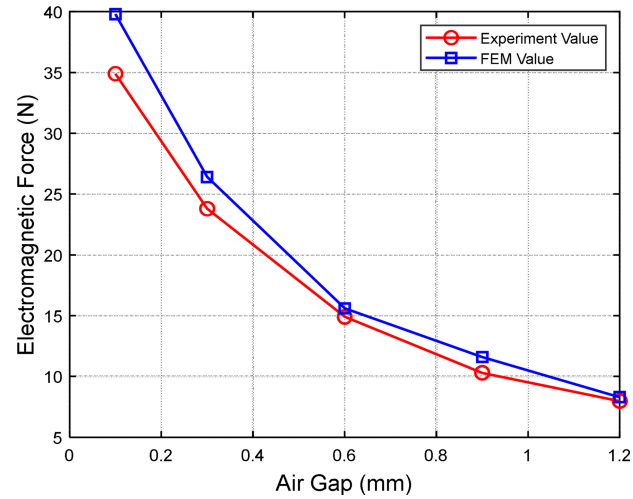

Fig. 11. Comparison of Electromagnetic Force-Air Gap Curve Experimental Values and Analysis Values

Table 4. Comparison of electromagnetic Experimental Values and Analysis Values

Air Gap	Experiment Value	FEM Value	Absolute Error	Relative Error
0.10 mm	34.9 N	39.8 N	4.90 N	14.0%
0.30 mm	23.8 N	26.4 N	2.60 N	10.9%
0.60 mm	14.9 N	15.6 N	0.70 N	4.69%
0.90 mm	10.3 N	11.6 N	1.30 N	12.6%
1.20 mm	7.98 N	8.30 N	0.32 N	4.01%

distribution around the air gap can be reasonably reproduced. Thus, when the geometry is close to axisymmetric, and the leakage is dominated by axisymmetric components, the discrepancy between FEM and experiment tends to decrease as the air gap increases [13].

Meanwhile, in the air gap region around (d) 0.90 mm, the absolute magnitude of the electromagnetic force is small; therefore, even an absolute error on the order of 1.30 N corresponds to a relatively large relative error of 12.6%, showing a tendency to increase compared with other air gap points except at (a) 0.1 mm and (b) 0.3 mm. However, this absolute error corresponds to about 3.2% of the maximum FEM-predicted force (approximately 39.8 N), and overall, the FEM results and experimental measurements show good qualitative agreement across the entire air gap range.

Accordingly, the FEM program used for electromagnetic field analysis and the analysis procedure employed in this study can be regarded as reliable, given that the difference between the simulated and measured forces remains within approximately 5 N. This trend is also consistent with previous reports indicating that modeling leakage flux as a separate magnetic reluctance element can significantly reduce discrepancies between magnetic circuit analysis and FEM results. Likewise, the FEM-experiment differences observed in this study support the conclusion that the primary sources of error are leakage flux and differences in three-dimensional flux distribution [14].

5. CONCLUSIONS

This paper analyzed how the electromagnetic force characteristics of a solenoid valve, as a function of air gap variation, affect the valve's actuation performance. First, the dynamic characteristics of the solenoid valve were examined through electromagnetic force experiments, and the results were then compared and analyzed by stroke condition using FEMM. The main conclusions drawn from the combined experimental measurements and FEM-based analyses are summarized as follows.

(1) As the air gap decreased (1.20 mm → 0.00 mm), the magnetic flux density increased nonlinearly, and the electromagnetic force also exhibited a nonlinear increasing trend. In contrast, during the air-gap-increasing interval (0.03 mm → 1.20 mm), the electromagnetic force measured at the same air gap was higher, confirming an asymmetric hysteresis behavior. This asymmetry was attributed to a dynamic hysteresis effect induced by eddy currents generated during the air gap transition process.

(2) A two-dimensional axisymmetric magnetostatic analysis using FEMM was conducted to obtain the flux density distribution under varying air gap conditions. As the air gap distance increased from (a) 0.10 mm to (e) 1.20 mm, the flux density decreased nonlinearly from 1.32 T to 0.50 T. This trend

is consistent with the general behavior that an increase in air gap raises the total magnetic reluctance of the magnetic circuit and increases fringing (leakage) flux, thereby reducing the magnetic flux produced under the same magnetomotive force. The electromagnetic-force-air-gap curve predicted by FEM also showed a qualitatively similar nonlinear decreasing trend to the experimental results, confirming that the proposed FEM model appropriately reproduces the air-gap-dependent electromagnetic force characteristics.

(3) The FEM-predicted forces were slightly higher than the experimental values, which is attributed to leakage flux effects in the housing and the plunger flow passages that were not included in the analysis model. Nevertheless, the difference between the two results remained within 5.00 N, indicating that the prediction accuracy is at a reliable level.

From Eq. (12), it can be confirmed that the braking force due to eddy currents is a function of the plunger velocity. Therefore, future work will investigate the dynamic hysteresis associated with eddy currents as a function of plunger speed in order to more precisely identify their influence on the electromagnetic force characteristics.

CRediT Authorship Contribution Statement

Min Jun Kim: Methodology, Validation, Writing the original draft. **Hwa Young Kim:** Review, Editing, Supervision.

Declaration of Competing Interest

The authors declare that they have no known competing financial interests or personal relationships that could have appeared to influence the work reported in this paper.

Acknowledgements

This work was supported by the National Research Foundation (NRF), Korea, under project BK21 FOUR (No. 412020 0313832).

REFERENCES

[1] S.N. Yun, Y. B. Ham, J.D. Jo, Understanding Solenoid Test Specifications, J. Korean Soc. Automot. Eng. 24 (2002) 64–68.
[2] J. Choi, J.H. Ahn, H.Y. Kim, Modeling the Dynamic Behavior of a Pilot-Operated Solenoid Valve for an Ultra-High Pressure Vessel, Appl. Sci. 11 (2021) 2329.
[3] L. Yang, T. Gao, X. Du, F. Zhai, C. Lu , X. Kong, Electromagnetic Characteristics Analysis and Structure Optimization of High-Speed Fuel Solenoid Valves, Machines 10 (2022) 964.
[4] H.-J. Park, H.-L. Kang, S.-H. Han, Evaluation of Attraction Forces due to Coil Heating of a Solenoid Valve for a Hydrogen Fuel Cell, J. Korean Soc. Manuf. Process Eng. 23 (2024) 111–117.
[5] M.-H. Yoon, Y.-Y. Choi, J.-P. Hong, Improvement in Thrust Force Estimation of Solenoid Valve Considering Magnetic Hysteresis, AIP Adv. 7 (2017) 056607.
[6] J. Akita, Solenoid Stroke Measurement Method Using Two Points of PWM Drive Current, IEEJ Trans. Electr. Electron. Eng. 20 (2025) 1608–1613.
[7] E. Düzgün, G. Şefkat, The Design and Analysis of a Proportional Solenoid with Experimental Validation of Static and Dynamic Behavior, Appl. Sci. 14 (2024) 11990.
[8] P. Liu, L. Fan, Q. Hayat, D. Xu, X. Ma, E. Song, Research on Key Factors and Their Interaction Effects of Electromagnetic Force of High-Speed Solenoid Valve, Sci. World J. 2014 (2014) 567242.
[9] P. Liu, R. Zhang, Q. Zhao, S. Peng, Eddy Effect and Dynamic Response of High-Speed Solenoid Valve with Composite Iron Core, Materials 16 (2023) 5823.
[10] J. Zhao, P. Yue, K. Wei, Eddy current effects on the dynamic response of high-speed solenoid valve for common rail injector, Int. J. Appl. Electromagn. Mech. 62 (2020) 607–618.
[11] H.R. Lee, J.H. Ahn, J.O. Shin, H.Y. Kim, Design of a Cylinder Valve Solenoid for a CNG Vehicle Using Electromagnetic Field Analysis, J. Korean Soc. Manuf. Process Eng. 15 (2016) 89–96.
[12] R.R. Chladny, C.R. Koch, A.F. Lynch, Modeling of Automotive Gas-Exchange Solenoid Valve Actuators, IEEE Trans. Magn. 41 (2005) 1155–1162.
[13] D. Meeker, Finite Element Method Magnetics (FEMM) Version 4.2 User's Manual, 2015. https://www.femm.info/Archives/doc/manual.pdf.
[14] S.J. Kim, W.Y. Kim, J.M. Lee, Y.C. Bae, Modeling of Flux Leakage in a Magnetic Circuit with Permanent Magnet, Trans. Korean Soc. Noise Vib. Eng. 21 (2011) 99–105.